Experimental implementation of a logical Bell state encoding

J. S. Hodges,[1] P. Cappellaro,[1,*] T. F. Havel,[1] R. Martinez,[2] and D. G. Cory[1]
[1]*Department of Nuclear Science and Engineering, Massachusetts Institute of Technology, Cambridge, Massachusetts 02139, USA*
[2]*Department of Chemistry, New Mexico Highlands University, Las Vegas, New Mexico 87701, USA*
(Received 5 November 2006; revised manuscript received 25 January 2007; published 18 April 2007)

Liquid-phase NMR is a general-purpose testbed for developing methods of coherent control relevant to quantum information processing. Here we extend these studies to the coherent control of logical qubits and in particular to the unitary gates necessary to create entanglement between logical qubits. We report an experimental implementation of a conditional logical gate between two logical qubits that are each in decoherence-free subspaces that protect the quantum information from fully correlated dephasing.

DOI: 10.1103/PhysRevA.75.042320 PACS number(s): 03.67.Pp, 76.60.−k, 33.25.+k

I. INTRODUCTION

Experimental implementations of quantum information processors have reached sufficient complexity that it is now possible to experimentally explore the avoidance and correction of quantum errors by encoding quantum information. These information encoding methods include active techniques, like quantum error-correcting codes (QECCs) [1–5] and dynamical decoupling [6–9], and passive techniques, such as decoherence-free subspaces (DFSs) [10–12], noiseless subsystems (NSs) [13], and topological schemes [14]. To date the ability to store information [15–19], to perform universal quantum operations [20], and to implement simple two-qubit algorithms within a variety of logical encodings [21,22] has been demonstrated.

Entanglement, a uniquely quantum resource, enables many of the speedups afforded by quantum information processing (QIP) including many-body physics simulations [23,24] exponential algorithmic enhancements [25], metrology [26], and communication [27]. Creation of entangled quantum states continues to drive experimental research in quantum information [28–31] and has served as a benchmark for coherent control. Here we combine the two concepts of logical qubits and entanglement creation to prepare a pseudopure version of a Bell state between logical qubits.

Control of encoded qubits must naturally respect the symmetries involved in the encoding. In the simplest case, this is achieved by having the control Hamiltonians commute with the noise generators [8]. When this is not experimentally possible or is inconvenient, high fidelity control is achievable via modulation schemes that limit the encoded information's excursion out of protected subsystems to times short compared to the noise correlation time [32].

This paper focuses on experimental implementations of the modulation sequences studied in [32] for creating entanglement among logical qubits, specifically creating a logical Bell state between a pair of DFS qubits immune to collective dephasing. Furthermore, we perform our entanglement creation gate on two distinct initial states: (i) a pseudopure state effectively pure over the entire four-qubit Hilbert space and (ii) a subsystem pseudopure state (see following paper [48]). We also give an analysis of the quantum state correlations given these two input states and identify the largest errors in implementing this gate.

II. LOGICAL BASIS ENCODING

Using the open quantum system approach, we model the total Hamiltonian of our system and environment as

$$\mathcal{H} = \mathcal{H}_S \otimes \mathbb{1}_E + \mathbb{1}_S \otimes \mathcal{H}_E + \mathcal{H}_{SE}, \tag{1}$$

where $\mathcal{H}_S$ is the nuclear spin system Hamiltonian, $\mathcal{H}_E$ is the environment Hamiltonian, and $\mathcal{H}_{SE}$ describes the system-environment coupling. For this example we choose an encoding for a simple noise model, collective σ_z noise, which corresponds to random fluctuations of the local magnetic field B_z. Defining the total angular momentum of the system as $J_z = \sum_{i=1}^{N} \sigma_z^i$, the interaction Hamiltonian is

$$\mathcal{H}_{SE} = \gamma J_z \otimes B_z. \tag{2}$$

The potential errors that the coupling to the magnetic fields can induce belong to the interaction algebra $\mathcal{A}_z = \{\mathbb{1}, J_z, J_z^2, \ldots, J_z^N\}$ [20]. In the two spin case ($N=2$), the eigenspace of the noise operator J_z with eigenvalue 0 is a $\mathbb{C}^2 \times \mathbb{C}^2$ decoherence-free subspace and can be used to encode one qubit of information. This DFS is thus spanned by the basis vectors $|01\rangle$ and $|10\rangle$. A natural encoding of a logical qubit $|\psi\rangle_L$ is given by

$$\alpha|0\rangle_L + \beta|1\rangle_L \Leftrightarrow \alpha|01\rangle + \beta|10\rangle. \tag{3}$$

The logical analogs of spin operators σ_x, σ_y, σ_z, and $\mathbb{1}$, which fully parametrize a single qubit, are

$$\sigma_z^L \Leftrightarrow \frac{\sigma_z^1 - \sigma_z^2}{2}, \quad \sigma_x^L \Leftrightarrow \frac{\sigma_x^1\sigma_x^2 + \sigma_y^1\sigma_y^2}{2},$$

$$\mathbb{1}^L \Leftrightarrow \frac{\mathbb{1}^{1,2} - \sigma_z^1\sigma_z^2}{2}, \quad \sigma_y^L \Leftrightarrow \frac{\sigma_x^1\sigma_y^2 - \sigma_y^1\sigma_x^2}{2}. \tag{4}$$

Furthermore, it will be convenient to describe conditional logic using the logical idempotent operators

$$E_\pm^L \Leftrightarrow \frac{\mathbb{1}_{L\pm}\sigma_z^L}{2} = \frac{\mathbb{1}^{1,2} - \sigma_z^1\sigma_z^2 \pm \sigma_z^1 \mp \sigma_z^2}{4}. \tag{5}$$

*Present address: ITAMP, Harvard-Smithsonian Center for Astrophysics, Cambridge, Massachusetts 02138, USA.

In the four-spin case ($N=4$) the J_z eigenspace with eigenvalue 0 is spanned by six basis vectors: $|0011\rangle$, $|0101\rangle$, $|0110\rangle$, $|1001\rangle$, $|1010\rangle$, and $|1100\rangle$. Any four of these states can span a $\mathbb{C}^4\times\mathbb{C}^4$ subspace containing two logical qubits of information. We chose the basis $|0101\rangle$, $|0110\rangle$, $|1001\rangle$, $|1010\rangle$. In addition to being immune to fully correlated dephasing under J_z, these states are also immune to pairwise collective dephasing under noise generators $j_z^{12}=\sigma_z^1+\sigma_z^2$ and $j_z^{34}=\sigma_z^3+\sigma_z^4$. The protected subspace is thus a tensor product space of two qubits of the form (3).

III. IMPLEMENTING ENTANGLEMENT CREATION GATES ON A QUANTUM SYSTEM

Given a fiducial state in the computational basis, applying a Hadamard gate and subsequently a controlled-NOT (CNOT) gate creates one of the four Bell states. The creation of a logical Bell state amounts to implementing logical versions of Hadamard and CNOT gates. The Hadamard gate on a logical qubit is specified, up to a global phase, as

$$iU_H = i\frac{\sigma_x^L+\sigma_z^L}{\sqrt{2}} = e^{-i(\pi/8)\sigma_y^L}e^{-i(\pi/2)\sigma_x^L}e^{i(\pi/8)\sigma_y^L}. \tag{6}$$

The unitary operator for implementing a CNOT gate can be decomposed into a product of unitary operators of the form of single logical spin rotations and couplings of the ZZ form:

$$U_{C_0\text{NOT}} = E_+^{1L}\sigma_x^{2L} + E_-^{1L}\mathbb{1}^{2L}$$

$$= e^{i(\pi/4)\mathbb{1}^{1L}\mathbb{1}^{2L}}e^{-i(\pi/4)\sigma_y^{2L}}e^{-i(\pi/4)(\sigma_z^{1L}+\sigma_z^{2L})}e^{-i(\pi/4)\sigma_z^{1L}\sigma_z^{2L}}e^{i(\pi/4)\sigma_y^{2L}}. \tag{7}$$

By expanding each of the exponentials above using the logical Pauli operators (4), many simplifications are possible. For instance, when a logical operator consists of a sum of commuting bilinear terms, it may suffice to drop all but one of the terms in the sum and add a constant scaling factor provided this simplified unitary has the same effect as the full unitary on a state within the logical encoding. One example is the isomorphism between a rotation of $\pi/2$ about σ_x^{1L} and a π rotation about $\sigma_x^1\sigma_x^2$ or $\sigma_y^1\sigma_y^2$:

$$e^{-i\theta(\sigma_x^1\sigma_x^2+\sigma_y^1\sigma_y^2)/2} = e^{-i\theta\sigma_x^1\sigma_x^2/2}e^{-i\theta\sigma_y^1\sigma_y^2/2}$$

$$= \left[\cos\left(\frac{\theta}{2}\right)\mathbb{1} - i\sin\left(\frac{\theta}{2}\right)\sigma_x^1\sigma_x^2\right]\left[\cos\left(\frac{\theta}{2}\right)\mathbb{1} - i\sin\left(\frac{\theta}{2}\right)\sigma_y^1\sigma_y^2\right]$$

$$= \cos^2\left(\frac{\theta}{2}\right)\mathbb{1} + \sin^2\left(\frac{\theta}{2}\right)\sigma_z^1\sigma_z^2 - i\sin(\theta)\frac{\sigma_x^1\sigma_x^2+\sigma_y^1\sigma_y^2}{2}$$

$$= {}^L\cos(\theta)\mathbb{1} - i\sin(\theta)(\sigma_+^1\sigma_-^2+\sigma_-^1\sigma_+^2), \tag{8}$$

$$e^{-i\theta\sigma_x^1\sigma_x^2} = \cos(\theta) - i\sin(\theta)\sigma_x^1\sigma_x^2$$

$$= \cos(\theta)\mathbb{1} - i\sin(\theta)(\sigma_+^1\sigma_+^2+\sigma_+^1\sigma_-^2+\sigma_-^1\sigma_+^2+\sigma_-^1\sigma_-^2)$$

$$= {}^L\cos(\theta)\mathbb{1} - i\sin(\theta)(\sigma_+^1\sigma_-^2+\sigma_-^1\sigma_+^2), \tag{9}$$

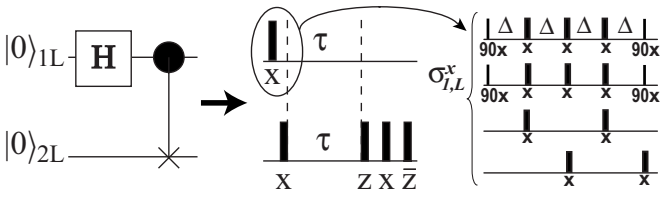

FIG. 1. From left to right: Entangling circuit on logical qubits and corresponding logical pulses and the pulse sequence implementing the σ_x^{1L} logical rotation on the physical qubits.

$$e^{-i\theta\sigma_y^1\sigma_y^2} = \cos(\theta) - i\sin(\theta)\sigma_y^1\sigma_y^2$$

$$= \cos(\theta)\mathbb{1} - i\sin(\theta)(-\sigma_+^1\sigma_+^2+\sigma_+^1\sigma_-^2+\sigma_-^1\sigma_+^2-\sigma_-^1\sigma_-^2)$$

$$= {}^L\cos(\theta)\mathbb{1} - i\sin(\theta)(\sigma_+^1\sigma_-^2+\sigma_-^1\sigma_+^2). \tag{10}$$

Here the last lines in (8)–(10) are all equivalent. The $=^L$ operation keeps only the terms that act within the logical subspace. Explicitly, the logical basis states are eigenstates of the $\sigma_z^1\sigma_z^2$ operator with eigenvalue -1; likewise, the eigenvalues of $\sigma_\pm^1\sigma_\pm^2$ are all zero. Using the following substitutions the net unitary of a Hadamard gate and a CNOT gate can be decomposed into four separate logical operations (up to a global, unobservable phase), each consisting of a $\pi/2$ rotation about a single bilinear term:

$$U_{C_0\text{NOT}}U_H \Leftrightarrow e^{i\varphi}U_4U_3U_2U_1, \tag{11}$$

$$U_1 = e^{-i(\pi/4)\sigma_y^1\sigma_y^2}, \quad U_2 = e^{-i(\pi/4)\sigma_y^3\sigma_y^4},$$
$$U_3 = e^{-i(\pi/4)\sigma_z^2\sigma_z^3}, \quad U_4 = e^{-i(\pi/4)\sigma_x^3\sigma_y^4} \tag{12}$$

The $\vec{\sigma}\cdot\vec{\sigma}$ interaction present in the internal Hamiltonian provides a means to perform σ_x^L rotations, but this is efficient only when the chemical shift differences ($|\omega_i-\omega_0|$) are suppressed. When the chemical shift differences are nonnegligible a Carr-Purcell (CP) style sequence can be used to engineer a $\vec{\sigma}\cdot\vec{\sigma}$ interaction [32,33]. By applying collective π rotations on a pair of spins comprising a logical bit, the chemical shift terms can be averaged to zero, retaining the ZZ term to first order. Staggered π rotations on the spins of the other logical bit are applied in a manner to refocus all operators in the Hamiltonian associated with these spins (see Fig. 1).

To generate a σ_x^{1L} coupling, we first generate the zeroth-order average Hamiltonian $\mathcal{Z}_{12}=(\pi/2)J_{12}\sigma_z^1\sigma_z^2$ [34,35] by employing a CP-like sequence:

$$\Delta_{12} - \pi|_x^{1,2,3} - \Delta_{12} - \pi|_x^{1,2,4} - \Delta_{12} - \pi|_x^{1,2,3} - \Delta_{12} - \pi|_x^4. \tag{13}$$

{Note the notation $\theta|_\mu^k \equiv \exp[-i(\theta/2)\Sigma_k\sigma_\mu^k]$.} The effective unitary propagator to zeroth order is $U^{(0)}=e^{-4i\Delta_{12}\mathcal{Z}_{12}}$.

By applying "collective" $\pi/2$ rotations about $\hat{x}$ before the above sequence and a $\pi/2$ rotation about $-\hat{x}$ after, the average Hamiltonian is transformed into $\sigma_y^1\sigma_y^2$ which has the same action as a σ_x^{1L}. Similarly, if the rotation axes are separated by $\pi/2$ (i.e., a $\hat{y}$-phased pulse on one of the spins in the logical pair and an $\hat{x}$-phased pulse on the other), an operator

isomorphic to σ_y^{1L} is achieved. The logical "two-body" interaction—$\sigma_z^{1L}\sigma_z^{2L}$—acting on the encoded subspaces is isomorphic to $\sigma_z^1\sigma_z^3$. We obtain this by using (13) and replacing spin 2 with spin 3. Each of the four rotations in (12) can be generated in this manner yielding an overall sequence

$$\left.\frac{\pi}{2}\right|_{\bar{x}}^{1,2} - \mathsf{Z}_{12} - \left.\frac{\pi}{2}\right|_{x}^{1,2,3,4} - \mathsf{Z}_{34} - \left.\frac{\pi}{2}\right|_{\bar{x}}^{3,4} - \mathsf{Z}_{23} - \left.\frac{\pi}{2}\right|_{x}^{3}\left.\frac{\pi}{2}\right|_{y}^{4} - \mathsf{Z}_{34} - \left.\frac{\pi}{2}\right|_{\bar{x}}^{3}\left.\frac{\pi}{2}\right|_{\bar{y}}^{4}, \tag{14}$$

where Z_{jk} denotes the subsequence generating $\mathcal{Z}_{jk}$ and setting $\Delta_{jk}=(2J_{jk})^{-1}$.

IV. EXPERIMENT

Our quantum system is comprised of the four ^{13}C spins $\left(I=\frac{1}{2}\right)$ of isotopically labeled crotonic acid (also known as trans-3-butenoic acid) [36]. This molecule contains nine magnetically active nuclei in total; the total spin system Hamiltonian takes the form

$$\mathcal{H}_{internal} = \frac{1}{2}\sum_{i\in \mathrm{C}}(\omega_i-\omega_0^{\mathrm{C}})\sigma_z^i + \frac{1}{2}\sum_{k\in \mathrm{H}}(\omega_k-\omega_0^{\mathrm{H}})\sigma_z^j + \sum_{i,j\in \mathrm{C};i<j}\frac{\pi}{2}J_{ij}\vec{\sigma}^i\cdot\vec{\sigma}^j + \sum_{k,l\in \mathrm{H};k<l}\frac{\pi}{2}J_{kl}\vec{\sigma}^k\cdot\vec{\sigma}^l + \sum_{j,k;j<k}\frac{\pi}{2}J_{jk}\sigma_z^j\sigma_z^k, \tag{15}$$

where ω_0^{C} (ω_0^{H}) is the rotating-frame frequency near the ^{13}C (^{1}H) Larmor frequency, the ω_i are the chemical shifts of the four carbon nuclear spins, the ω_k are the chemical shifts of the five hydrogen nuclear spins, and the six J_{ij} (ten J_{kl}) are the scalar coupling constants between two carbon (two hydrogen) spins (as usual, $\hbar=1$). We are mainly concerned with coherently controlling the carbon subsystem of spins and seek to suppress the proton subsystem. As the heteronuclear scalar couplings (terms $J_{j,k}$) are the only means of mixing the two subsystems, a broadband decoupling sequence modulating the proton spin system effectively removes this coupling during the experiment. In practice, decoupling the proton spin system is equivalent to saturating the populations of the proton spins. One potential artifact of this approach is the introduction of transient nuclear Overhauser effects [37–40].

A. Pseudopure states over the entire Hilbert space

Starting with the equilibrium density matrix of the four-spin system, $\rho\approx\mathbb{1}/N-\epsilon(\Sigma_j^N\sigma_z^j)$, we prepared our system in the dual DFS ground state $|0101\rangle=|00\rangle_L$ using spatial averaging techniques [41,42]. As shown in Fig. 2, the preparation of the encoded logical state is complex and requires a preparation time of 0.1186 s relative to the total experiment length of 0.1662 s. The T_2's of the carbons are all greater than 500 ms [43] and therefore spin-spin relaxation is unimportant over the length of the experiment. Since pseudopure-state preparation is a nonunitary, completely positive map, a loss of observable signal is expected. In our implementation of pseudopure-state preparation the signal is roughly 2/13 that of the equilibrium state.

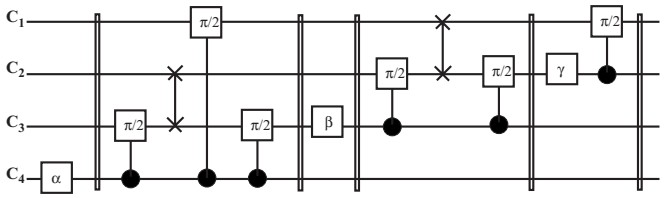

FIG. 2. Circuit for the preparation of the pseudopure state. We represent single-qubit rotations by square boxes; controlled rotations by closed circles on the controlling qubit linked to the applied rotation on the controlled qubit; SWAP gates by two crosses on the swapped qubits, connected by a vertical line; nonunitary operations (gradients) by double vertical bars. Notice the number of controlled operations, each requiring a time of the order of the inverse coupling strength, and SWAP gates, each requiring three times the inverse coupling strength. The single-qubit rotations above have the values $\alpha\approx 9/20\pi$, $\beta\approx 2/5\pi$, and $\gamma\approx 2/7\pi$ which account for the scaling of the signal-to-noise compared to the equilibrium state.

All qubit rotations (selective, semiselective, or collective for all spins) were created using robust strongly-modulating pulses (SMPs) [44,45] by maximizing the gate fidelity of the ideal propagator to the simulated propagator. Furthermore, as the radio frequency (rf) control fields are inhomogeneous over the sample, we maximize the effective gate fidelity, averaging over a weighted distribution of rf field strengths. Pulse lengths for this system range from 200 to 800 μs; the simulated gate fidelities for any individual pulse are greater than 0.99%. The dominant source of residual errors in a typical SMP come from two-body terms of the form $\sigma_\mu^j\sigma_\nu^k$. After many pulses these small residual errors accumulate, but the net effect can be partially suppressed by adjusting the delay time between pulses [46] to optimize the overall gate fidelity or state correlation. The required $\pi/2$ rotations about the logical operator axes were obtained by implementing the sequence in (13) and setting $\Delta_{jk}=1/2J_{jk}$. In principle, we would like to repeat the sequence N times and scale Δ by a factor of $1/N$ in order to induce a rapid refocusing of the noise; however, in practice Δ is limited by the length of the semiselective pulses. For all of the logical rotations implemented experimentally, we use $N=1$.

The density matrices of the spin system after the initial pseudopure preparation and after the entanglement creation were reconstructed using state tomography [47], which involves applying 18 readout pulses to obtain coefficients for the 256 operators comprising a complete operator basis of the four spin-$\frac{1}{2}$ ^{13}C nuclei.

B. Subsystem pseudopure states

As shown in the following paper [48], for mixed-state ensemble quantum information processing there are advantages to requiring the initial state to be pure only over the subsystem containing the relevant quantum information. Here we implement the entangling operation over logical qubits using the double DFS initial state described in [48].

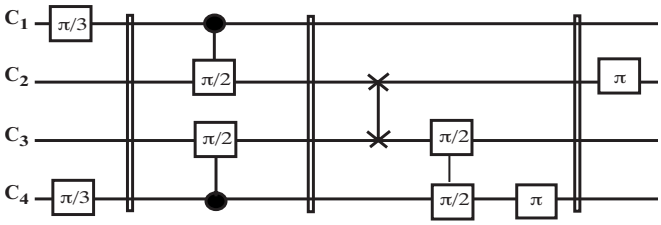

FIG. 3. Circuit for the preparation of the subsystem pseudopure state. We use the same convention as in Fig. 2.

This state (Fig. 3) can be prepared in half the time of the full pseudopure state (0.0568 s) and has a smaller loss of signal (2/3 compared to 2/13).

C. Density matrix reconstruction

The reconstructed density matrices are shown in Figs. 4 and 5, where the vertical axes show the normalized amplitude and the horizontal axes label the basis states in the computational basis (i.e., $|0000\rangle$,$|0001\rangle$,…). The effects of decoherence while performing the entangling operation can be qualitatively seen in the final state as an attenuation of the off-diagonal terms of the Bell state $(|01\rangle_L+|10\rangle_L)/\sqrt{2}$. Such attenuation does not alter this state's protection against collective dephasing. Also, we note that this particular Bell state $[(|01\rangle+|10\rangle)/\sqrt{2}]$ is immune to collective dephasing under the noise generator j_z^{12} but the Bell states $(|00\rangle\pm|11\rangle)/\sqrt{2}$ are not.

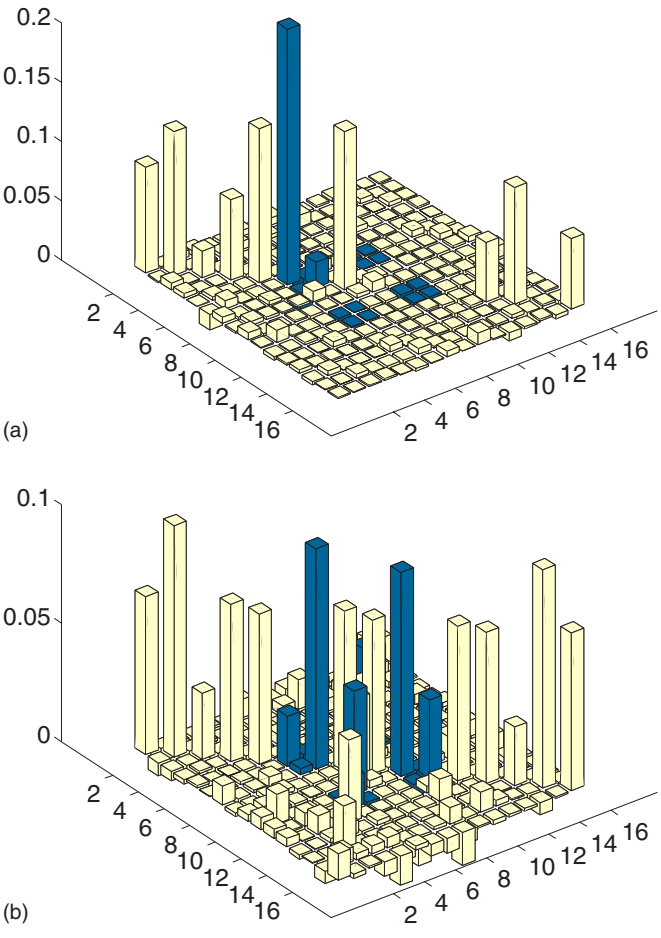

FIG. 4. (Color online) Density matrices for the initial pseudopure state over only the logical subspace (a) and the corresponding Bell state (b). The darker part indicates the states in the logical subspace. In the case of the subsystem pseudopure states, the division of the logical subspace allows for the other areas of Hilbert space to be mixed.

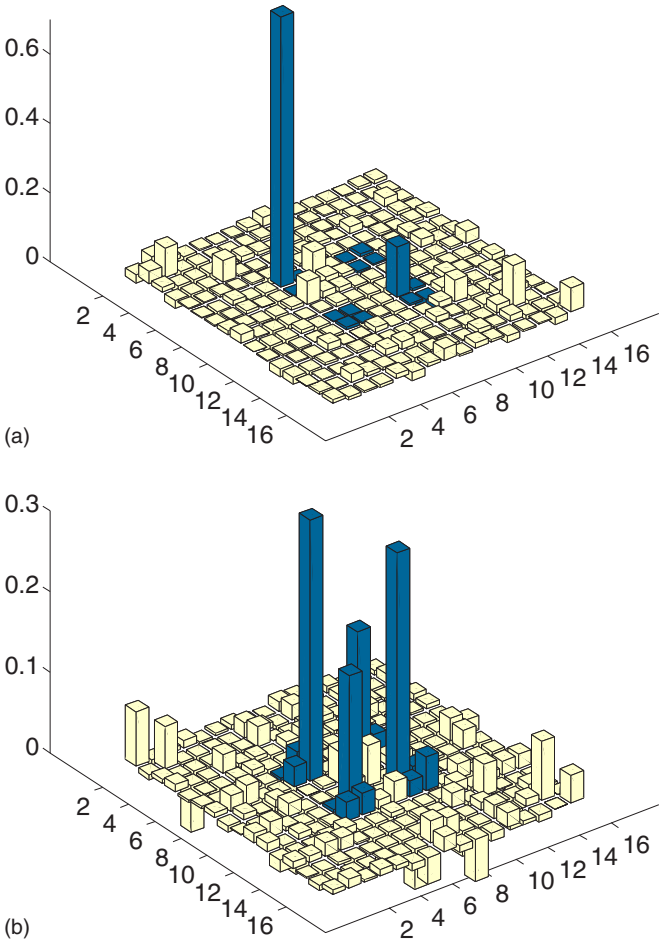

FIG. 5. (Color online) Density matrices for the initial pseudopure state over the entire Hilbert space (a) and the corresponding logical Bell state (b). The basis states comprising the dual DFS have been darkened.

V. DISCUSSION

Metrics of control

The quantum process associated with the encoded entangling operation can be specified by the general map

$$\mathcal{E}(\rho) = \sum_{\mu} A_{\mu} \rho A_{\mu}^{\dagger}, \tag{16}$$

where A_μ are Kraus operators describing the experimental implementation of the encoded operation, and ρ is defined over the entire Hilbert space. If the process consists of strictly coherent dynamics a single Kraus operator defines

the operation: $A_0=U$. The correlation of two quantum states is defined as

$$C=\frac{\mathrm{Tr}(\rho_{id}\rho_{expt})}{\sqrt{\mathrm{Tr}(\rho_{id}^2)\mathrm{Tr}(\rho_{expt}^2)}} \tag{17}$$

which defines the relative closeness of states in Hilbert space with proper normalization. Here $\rho_{id}=U\rho_{in}U^\dagger$, $\rho_{expt}=\mathcal{E}(\rho_{in})$, and ρ_{in} define the ideal, experimental, and input states, respectively. The closeness of the ideal state to the experimental state measures how well we have implemented the logical entangling operation for a particular input state.

When the quantum process $\mathcal{E}$ includes incoherent and decoherent dynamics, the purity $[\mathrm{Tr}(\rho^2)]$ of the experimental state ρ_{expt} is less than that of the initial state ρ_{in}. In this case, one can define an attenuated correlation $C'=\gamma C$ where the attenuation coefficient is defined as

$$\gamma=\sqrt{\frac{\mathrm{Tr}(\rho_{expt}^2)}{\mathrm{Tr}(\rho_{in}^2)}}. \tag{18}$$

When the relevant quantum information resides only in a subspace, we can also measure the correlation inside this subspace by applying the projectors spanning the subspace (P_L) to the state [48]

$$C_{LL}(\rho)=\frac{\mathrm{Tr}(P_L\rho_{th}P_L\sum_\mu A_\mu P_L\rho_{in}P_L A_\mu^\dagger)}{\sqrt{\mathrm{Tr}[(P_L\rho_{in}P_L)^2]\mathrm{Tr}[(P_L\rho_{th}P_L)^2]}}. \tag{19}$$

This measure is important when creating subsystem pseudopure states, where nonzero contributions to the density operator outside the logical subspace contribute to C. The logical subspace correlation C_{LL} is identical to the full Hilbert space correlation C provided that $\rho_{in}=P_L\rho_{in}P_L$ and $\rho_{id}=P_L\rho_{id}P_L$, which should be the case for a full pseudopure state (FPPS).

Since the experimental implementation of the pulse sequence used to generate logical entanglement is independent of the initial state, we can use both initial states and the aforementioned measures to gauge our control of the logical subspace. When these measures differ with different initial states we reveal several key features of the experimental implementation not accounted for in the simulation.

With respect to a simulation of the NMR system over four spins, the sequence generates the desired logical entanglement with high fidelity regardless of initial state. For example, in comparing the full pseudopure state and the subsystem pseudopure state (SPPS), we see that the correlation between the ideal state and the simulated state (C_{sim}) are nearly unity and differ from each other by only 1%. The resulting simulated correlations of the full and subsystem pseudopure Bell states (FPPBS and SPPBS, respectively), also differ by only 1% and are quite close to unity. Last, the attenuation coefficients differ by 2%. As the simulations do not take into account any decoherent or relaxation processes (T_1, T_2, Overhauser effects, etc.) any reduction in purity is due solely to the simulation of rf inhomogeneity, an incoherent process.

TABLE I. Experimental and simulated data for the implementation of the encoded Bell state propagator. Experimental errors of $\approx$4% can be attributed to systematic errors in the fitting algorithm used to reconstruct the density matrix from NMR spectral data. C_{sim} represents the correlation between simulation of the NMR spin system and the ideal state, taken over the entire Hilbert space. C_{expt} compares this same simulation of the experiment to the experimental tomography reconstruction of the state, in the entire Hilbert space. C_{LL} measures the correlation between the simulated and experimental states projected onto the logical subspace.

Quantum state	C_{sim}	C_{expt}	c_{LL}
Full pseudopure state	0.98	0.91	0.99
Full pseudopure Bell state	0.96	0.74	0.95
Subsystem pseudopure state	0.99	0.97	0.99
Subsystem pseudopure Bell state	0.97	0.87	0.91

In comparing the experimentally measured density operator with the simulations we can quantify our ability to experimentally create the desired initial state, implement our entangling operation, and see the effects of decoherence on the system. First, we see that the correlation of the SPPS is 6% higher than that of the FPPS when measured over the entire Hilbert space (C_{expt}) but equal and nearly unity when the states are projected onto the logical subspace (C_{LL}). This apparent discrepancy represents errors due to unwanted, nonzero contributions to the density operator *outside* the logical subspace since $C_{expt}=\Sigma_{jk}\alpha_{jk}C_{jk}$ where C_{jk} represent correlations for blocks of the density operator and α is a weighting factor summing to unity $(\Sigma_{jk}\alpha_{jk}=1)$ [48]. To illustrate this aspect, we can calculate C_{RR}, α_{LL}, and α_{RR} for both initial states (see Tables I and II).

For the SPPS, $C_{RR}=0.97$, $\alpha_{LL}=0.38$, and $\alpha_{RR}=0.61$. Whereas for the FPPS, $C_{RR}=0.45$, $\alpha_{LL}=0.89$, and $\alpha_{RR}=0.05$. (For the ideal SPPS α_{LL} should be 4/9 and α_{RR} should be 5/9; for the ideal FPPS α_{LL} should be 1.) The C_{expt} value for the SPPS is much higher than that of the FPPS due to having near unit values for both C_{RR} and C_{LL} and $\alpha_{LR}\approx 0$. Physically, this emphasizes the advantages of using a simpler initial state. For the FPPS we must create a total density operator with equal weightings of the many-spin correlations like $\sigma_z^1\sigma_z^2\sigma_z^3\sigma_z^4$ and all the combinations of $\sigma_z^1\sigma_z^2\sigma_z^3$

TABLE II. Attenuation coefficients for encoded Bell states. These values represent a loss of purity in implementing a sequence of gates for entangling logical qubits. γ_{sim} shows the attenuation of the ideal encoded Bell state of a NMR simulation including coherent and incoherent processes only, normalized to the initial-state purity. γ_{expt} shows the loss of purity between the experimental initial state and final states, reconstructed using state tomography. γ_{LL} shows the loss of purity for the projection of these experimentally reconstructed states onto the logical subspace. Values less than unity indicate a loss of coherence in the spin system.

Quantum state	γ_{sim}	γ_{expt}	γ_{LL}
Full pseudopure Bell state	0.97	0.78	0.65
Subsystem pseudopure Bell state	0.95	0.87	0.72

between four spins starting from the thermal state: $\Sigma_{j=1}^{4}\sigma_z^j$. In the SPPS only terms involving classical correlations between two spins (like $\sigma_z^1\sigma_z^3$) are necessary. The primary source of error in creating pseudopure states over the entire Hilbert space are these many-spin correlations of the initial state, thus accounting for the lower C_{RR} contribution to the FPPS.

Next, we address our ability to experimentally implement encoded quantum operations by analyzing the different correlations of the FPPBS and the SPPBS. Since we use exactly the same pulse sequence to transform the FPPS to the FPPBS as we do for transforming the SPPS to the SPPBS, we would naively suspect the trends for the initial states to follow for the logical Bell states. However, the correlation between the experiment and the simulation for the SPPBS is roughly 18% better than that of the FPPBS. The fact that the FPPS and the SPPS are different states within the entire Hilbert space accounts for this: contributions from C_{RR} improve C_{expt} for subsystem pseudopure states. By calculating the projected correlations and weighting factors, we see that C_{expt} for the SPPBS is bolstered by C_{RR}, as $C_{RR}=0.91$, $\alpha_{RR}=0.64$, and $\alpha_{LL}=0.31$. For the FPPBS, $C_{RR}=0.41$, $\alpha_{RR}=0.06$, and $\alpha_{LL}=0.74$; as with the full pseudopure initial state, small errors outside the logical subspace considerably decrease the correlation over the entire Hilbert space. Furthermore, the pulse sequence seems to favor the SPPS state, as the purity (γ_{expt}) of the SPPBS is larger than the FPPBS. Again, this behavior indicates the presence of many-spin correlations in full pseudopure states, as these correlations can develop extended and fragile quantum coherences, decohering faster than a single spin or a single logical qubit.

Finally, if we consider the evolution in the logical subspace only, we find that C_{LL} is quite high for both the FPPBS and the SPPBS: 0.95 compared to 0.91, respectively. Though slightly different from the simulations, the two states are comparable as the correlation within the logical subspace between the experimentally measured FPPBS and the experimentally measured SPPBS is 0.97. This indicates that our control sequence will transform information within the logical subspace in a nearly identical manner, unbiased toward the information outside the logical subspace. In summary, we see that for a given implementation of the logical entangling operation, we can learn about the experimental imperfections by preparing two states that are both pure within a given subspace but each different outside of this subspace. In particular, when considering the loss of purity and the correlation with the logical subspace, a subsystem pseudopure state outperforms a full pseudopure state when comparing the measured initial and final states to simulations.

VI. CONCLUSION

Using a two-physical qubit encoding which protects against collective dephasing, we have shown how to implement quantum gates between logical qubits using effective Hamiltonians. It is important to stress that when selecting a protection scheme against decoherence the ability to encode a physical qubit into a logical qubit with high fidelity is not sufficient for computation. While we have demonstrated control over a pair of logical qubits, the coding we have chosen is not particularly relevant to the actual noise generators of our physical qubits. This example should be seen as an instance of NMR as a testbed for quantum information processing. The logically encoded Bell state actually decoheres faster than would the equivalent Bell state between two of the physical spins in our system.

The structure of the external and natural Hamiltonian plays an important role in the control of logical qubits, as the operators needed to implement gates may not be present and generating them may drive the information out of the subsystem. For large systems with significant symmetry (like quantum dots under the exchange interaction [49]) or exceedingly small systems [20], the structure of the natural Hamiltonian can provide the logical operations in itself. However, for systems of intermediate size (most relevant to the present implementations of quantum information processors) implementing quantum gates among logical qubits requires both a precise knowledge of the natural Hamiltonian and a complete set of control parameters to ensure no leakage from the protected subsystem or subspace. For example, if our four-qubit system were composed of two proton spins and two carbon spins, each individual species could be modulated separately, thus doubling the number of control parameters in the external Hamiltonian and limiting the leakage of the information from the subspace.

Our selection of logical qubits comprised of only two physical qubits limits our logical operations for single qubit and two-qubit interactions to only "two-body" operators. If instead we were to attempt a repetition of the experiment where the logical qubits were encoded under the three-qubit noiseless subsystem [16], the single-qubit and two-qubit rotations would involve "three-body" operators [50]—quite unlikely to be found in a natural Hamiltonian. In such a scenario, the ability to implement logical operations would necessarily need to come from a modulation sequence, appropriately chosen to avoid leakage from the subsystem.

ACKNOWLEDGMENTS

This work was supported in part by the National Security Agency (NSA) under Army Research Office (ARO) Contract No. W911NF-05-1-0469 and No. DAAD19-01-1-0519, by the Air Force Office of Scientific Research, and by the Quantum Technologies Group of the Cambridge-MIT Institute. The authors would like to thank N. Boulant for useful discussions.

[1] P. W. Shor, Phys. Rev. A **52**, R2493 (1995).
[2] A. R. Calderbank and P. W. Shor, Phys. Rev. A **54**, 1098 (1996).
[3] D. Gottesman, Phys. Rev. A **54**, 1862 (1996).
[4] A. M. Steane, Proc. R. Soc. London, Ser. A **452**, 2551 (1996).
[5] A. M. Steane, Phys. Rev. Lett. **77**, 793 (1996).
[6] L. Viola and S. Lloyd, Phys. Rev. A **58**, 2733 (1998).
[7] L. Viola, S. Lloyd, and E. Knill, Phys. Rev. Lett. **83**, 4888 (1999).
[8] L. Viola, E. Knill, and S. Lloyd, Phys. Rev. Lett. **82**, 2417 (1999).
[9] L. Viola, Phys. Rev. A **66**, 012307 (2002).
[10] P. Zanardi and M. Rasetti, Phys. Rev. Lett. **79**, 3306 (1997).
[11] L.-M. Duan and G.-C. Guo, Phys. Rev. Lett. **79**, 1953 (1997).
[12] D. A. Lidar, I. L. Chuang, and K. B. Whaley, Phys. Rev. Lett. **81**, 2594 (1998).
[13] E. Knill, R. Laflamme, and L. Viola, Phys. Rev. Lett. **84**, 2525 (2000).
[14] A. Y. Kitaev, Ann. Phys. (N.Y.) **303**, 2 (2003).
[15] P. G. Kwiat, A. J. Berglund, J. B. Altepeter, and A. G. White, Science **290**, 498 (2000).
[16] E. M. Fortunato, L. Viola, M. A. Pravia, E. Knill, R. Laflamme, T. F. Havel, and D. G. Cory, Phys. Rev. A **67**, 062303 (2003).
[17] D. Kielpinski, V. Meyer, M. A. Rowe, C. A. Sackett, W. M. Itano, C. Monroe, and D. J. Wineland, Science **291**, 1013 (2001).
[18] H. Haffner *et al.*, Appl. Phys. B: Lasers Opt. **81**, 151 (2005).
[19] C. Langer *et al.*, Phys. Rev. Lett. **95**, 060502 (2005).
[20] E. Fortunato, L. Viola, J. Hodges, G. Teklemarian, and D. Cory, New J. Phys. **4**, 5.1 (2002).
[21] M. Mohseni, J. S. Lundeen, K. J. Resch, and A. M. Steinberg, Phys. Rev. Lett. **91**, 187903 (2003).
[22] J. E. Ollerenshaw, D. A. Lidar, and L. E. Kay, Phys. Rev. Lett. **91**, 217904 (2003).
[23] R. Feynman, Found. Phys. **16**, 507 (1986).
[24] S. Lloyd, Science **273**, 1073 (1996).
[25] P. W. Shor, in *Proceedings of the 35th Annual Symposium on Foundations of Computer Science, 1994* (IEEE Computer Society Press, Sante Fe, New Mexico, 1994), pp. 124–134.
[26] P. Cappellaro, J. Emerson, N. Boulant, C. Ramanathan, S. Lloyd, and D. G. Cory, Phys. Rev. Lett. **94**, 020502 (2005).
[27] C. H. Bennett and G. Brassard, in *Proceedings of IEEE International Conference on Computers, Systems and Signal Processing, 1984* (IEEE, New York, 1984), pp. 175–179.
[28] C. Negrevergne, T. S. Mahesh, C. A. Ryan, M. Ditty, F. Cyr-Racine, W. Power, N. Boulant, T. Havel, D. G. Cory, and R. Laflamme, Phys. Rev. Lett. **96**, 170501 (2006).
[29] J.-S. Lee and A. K. Khitrin, Phys. Rev. A **70**, 022330 (2004).
[30] D. Leibfried *et al.*, Nature (London) **438**, 639 (2005).
[31] H. Haffner *et al.*, Nature (London) **438**, 643 (2005).
[32] P. Cappellaro, J. S. Hodges, T. F. Havel, and D. G. Cory, J. Chem. Phys. **125**, 044514 (2006).
[33] H. Carr and E. Purcell, Phys. Rev. **94**, 630 (1954).
[34] U. Haeberlen and J. S. Waugh, Phys. Rev. **175**, 453 (1968).
[35] U. Haeberlen, *High Resolution NMR in Solids: Selective Averaging* (Academic Press, New York, 1976).
[36] E. Knill, R. Laflamme, R. Martinez, and C.-H. Tseng, Nature (London) **404**, 368 (2000).
[37] A. W. Overhauser, Phys. Rev. **91**, 476 (1953).
[38] A. W. Overhauser, Phys. Rev. **92**, 411 (1953).
[39] T. Carver and P. Slicher, Phys. Rev. **92**, 212 (1953).
[40] I. Solomon, Phys. Rev. **99**, 559 (1955).
[41] D. Cory, M. Price, and T. Havel, Physica D **120**, 82 (1998).
[42] D. G. Cory, A. F. Fahmy, and T. F. Havel, Proc. Natl. Acad. Sci. U.S.A. **94**, 1634 (1997).
[43] N. Boulant, T. F. Havel, M. A. Pravia, and D. G. Cory, Phys. Rev. A **67**, 042322 (2003).
[44] E. Fortunato, M. Pravia, N. Boulant, G. Teklemariam, T. Havel, and D. Cory, J. Chem. Phys. **116**(17), 7599 (2002).
[45] M. A. Pravia, N. Boulant, J. Emerson, A. Farid, E. M. Fortunato, T. F. Havel, R. Martinez, and D. G. Cory, J. Chem. Phys. **119**, 9993 (2003).
[46] E. Knill, R. Laflamme, R. Martinez, and C. H. Tseng, Nature (London) **404**, 368 (2000).
[47] I. L. Chuang, N. A. Gershenfeld, M. G. Kubinec, and D. Leung, Proc. R. Soc. London, Ser. A **454**, 447 (1998).
[48] P. Cappellaro, J. S. Hodges, T. F. Havel, and D. G. Cory, following paper, Phys. Rev. A **75**, 042321 (2007).
[49] D. DiVincenzo, D. Bacon, J. Kempe, G. Burkard, and K. B. Whaley, Nature (London) **408**, 339 (2000).
[50] C. H. Tseng, S. Somaroo, Y. Sharf, E. Knill, R. Laflamme, T. F. Havel, and D. G. Cory, Phys. Rev. A **61**, 012302 (1999).